SUPPLEMENT SERIES

Astron. Astrophys. Suppl. Ser. **124,** 597-614 (1997)

CESAM: A code for stellar evolution calculations

P. Morel

Cassini, URA CNRS 1362 and GDR CNRS G 131, Observatoire de la Côte d'Azur, Nice, France

Received March 14, accepted December 6, 1996

Abstract. The code CESAM is a consistent set of programs and routines which performs calculations of 1D quasi-static stellar evolution including diffusion and rotation. The principal new feature is the solution of the quasi-static equilibrium by collocation method based on piecewise polynomials approximations projected on their B-spline basis; that allows stable and robust calculations and the exact restitution of the solution not only at grid points. Another advantage is the monitoring by only one parameter of the accuracy and its improvement by superconvergence. An automatic mesh refinement has been designed for adjusting the localizations of grid points according to the changes of unknowns, each limit between a radiative and a convective zones being shifted to the closest grid point. For standard models, the evolution of the chemical composition is solved by stiffly stable schemes of orders up to four; for non-standard models the solution of the diffusion equation employs the Petrov-Galerkin scheme, with the mixing of chemicals in convective zones performed by strong turbulent diffusion. A precise restoration of the atmosphere is allowed for. CESAM computes evolution of stars from the pre-main sequence to the beginning of the ^{4}He burning 3α cycle. In this paper a detailed description of the algorithms is presented.

Key words: methods: numerical — Sun: evolution — Sun: interior — stars: evolution — stars: interior

1. Introduction

The endeavor of a numerical code of stellar evolution is, more or less, directed towards a given goal; either the purpose is the computation of models evolved for long time intervals as for the study of AGB stages (Han et al. 1994), in which cases the search of efficient and low-cost algorithms is the priority, or a high level of accuracy has to be reached, as for solar models which need high numerical accuracy in addition to precise physics (Christensen-Dalsgaard 1982; Reiter et al. 1994).

Send offprint requests to: morel@obs-nice.fr

A first way for improving the numerical precision of a stellar model is the refinement of the mesh, a second is the use of a numerical algorithm of high order. Until recently the codes used for stellar evolution were, more or less, derived from the Henyey's code (Henyey et al. 1959, 1964) which uses finite differences and so, have a *fixed* order of accuracy, e.g. first or second; with this class of schemes, the only way to have various orders of accuracy is to write several algorithms.

For the integration of two-point boundary value problems, high accuracy (typically 10^{-10} or even better) can be obtained with the multishooting technique (Stoer & Bulirsch 1979, Sect. 7.3.5) employed in few codes of stellar evolution (Wilson 1981; Reiter et al. 1994). They are CPU consuming as reported by Embarek (1989) but they are well designed for parallel computers (Reiter et al. loc. cit.). Solar models with such impressive numerical accuracy have been calculated with a very few number ($\lesssim 50$) of fitting points. These methods, however, suffer of a conceptual gap between the reachable accuracy in space and in time since the mixing of the chemical species in Convective Zones (CZ) with such high-accuracy schemes is, in practice, only possible if neither thermonuclear reactions nor diffusion take place in CZ; therefore they are well suited for the calculation of Standard Solar Models (SSM). Applications of solar models are the computation of the eigenfrequencies; that needs a precise knowledge of the solution around the nodes whose locations change according to the modes, their orders and degrees; therefore the solution needs to be restored at locations well distributed around the turning points, i.e., between the grid points, that needs lengthy calculations with multishooting methods if the *full accuracy* is preserved.

The goal of CESAM[1] is to perform a standard solar evolution from ZAMS to present age with an accuracy of the order of 10^{-4}, using about 500 mass shells and 50 time steps (with a maximum time step of 100 million years); according to the physics employed it also calculates evolution from PMS to the onset of ^{4}He burning for various stellar masses. The method of integration does

[1] This acronym means: Code d'Evolution Stellaire Adaptatif et Modulaire.

not use the familiar finite differences; it is based on the so-called splines collocation method derived by de Boor (1978, Chapt. XVII). The basic idea is to seek piecewise polynomials as solutions of differential problems; among all the bases of the linear space of piecewise polynomials, the B-splines basis (de Boor, loc. cit.; Schumaker 1981) has been designed especially for calculation purposes. Its main advantages are: (i) the order of the scheme has only one parameter dependence, (ii) algorithms specially derived for spline calculations allow efficient and stable computations, (iii) a convenient method has been designed for connecting the pieces of polynomials with a given order of continuity, (iv) only few changes in the algorithms allow to get either the weak solutions (Galerkin's methods) or the strong solutions (collocation method), (v) ability of restoring exactly the numerical solution anywhere, (vi) ability to handle discontinuous solution, (vii) no need of a peculiar algorithm at the center. However, due to the non-trivial and unfamiliar algebra of B-splines, the algorithms are much more intricate than with the standard finite differences. With the use of a functional basis (i.e. presently, the B-spline basis) it is a triviality to structure the code in a "numerical space" where the differential problem is formally solved and in a "physical space" where the equations are formed whatever the numerical method used for their solution is; hence all the physics: Equation Of State (EOS), opacities, nuclear reaction rates, external boundary conditions, calculation of the convective flux, etc... are calculated in *external* routines which can be, on need, user supplied or taken from the source itself without any change in the "numerical space". Hence CESAM allows calculations of stellar models with various physical assumptions, physical data, external boundary conditions, numerical methods and numerical accuracy; it also includes diffusion and mass loss.

For consistency the same order of accuracy in time and in space is desirable; with respect to time, the fourth order is a hardly reachable upper limit, that is due to (i) the stiffness of the problem: the evolutionary time scales of the various chemical species differ by more than eighteen orders of magnitude, (ii) the convective mixing can hardly be done with a high order scheme. For standard models, i.e., without diffusion, the numerical scheme currently employed is the first order Euler's backward formulae (Kippenhahn et al. 1968), with simplifications (Arnett & Truran 1969) or improvements (Wagoner 1969), (Christensen-Dalsgaard 1982) makes use of the second order trapezoidal rule; CESAM uses a stiffly stable Implicit Runge Kutta (IRK) scheme with order up to 4. With diffusion, Runge Kutta scheme (Alecian 1986), finite difference schemes (Cox et al. 1989), Crank Nicholson (Proffit & Michaud 1991; Charbonel et al. 1992) are employed; in CESAM the diffusion and thermonuclear equations, with mixing of chemicals in CZ, are solved as a whole using the implicit backward first order Euler's scheme in time and, in space, the Petrov-Galerkin's method with order up to four.

Some recent papers are based on calculations made with CESAM (Morel et al. 1990; Morel et al. 1993, 1994; Berthomieu et al. 1993; Goupil et al. 1993; Audard & Provost 1994; Lebreton et al. 1995; Chmielewski et al. 1995; Morel & Schatzman, 1996). Preliminary and short descriptions of the numerical methods have already been given (Morel 1989; Morel 1993a, 1993b) or referenced (Gabriel 1990); the algorithms have been adapted for the computation of evolution of giant planets (Guillot & Morel 1995). This paper is devoted to a detailed description of the numeric of CESAM.

In Sect. 4 the basic physics of stellar evolution is briefly recalled for references and notations; special emphasis is given to the mixing of CZ, on initial conditions and on external boundary conditions for which a detailed restoration of an atmosphere is allowed for. Sect. 3 is devoted to the numerical techniques; a first part is concerned with the solution of the two points boundary problem with emphasis on the choice of the integration variables and on the automatic location of grid points; in a second part, the schemes used for solving the stiff differential initial value problem of the evolution of the chemical composition with, and without, diffusion are described. In Sect. 4 some indications concerning the management of the code are given. Results of investigations on internal accuracy are presented in Sect. 5 and the discussion in Sect. 6. Three appendices are devoted to numerical technical discussions.

1.1. Contents of the paper

2. Physical description

2.1. The equations for stellar evolution

Although several physical laws and data are more easily derived from the set of variables of state $\{\rho, T, \mathcal{X}\}$ (i.e. density, temperature, vector of the abundances of chemical species), with the numerical techniques employed, the set $(P, T, \mathcal{X})$ is more suitable[2]; P is the pressure.

Let, as independent lagrangian variable, M be the mass inside the sphere of radius R; at first order for the rotation, in the assumption of spherical symmetry, without magnetic field, the system of 1D rotating stellar structure equations:

$$\begin{cases} \frac{\partial P}{\partial M} = -\frac{GM}{4\pi R^4} + \frac{\Omega^2}{6\pi R} \\ \frac{\partial T}{\partial M} = \frac{\partial P}{\partial M}\frac{T}{P}\nabla \\ \frac{\partial R}{\partial M} = \frac{1}{4\pi R^2 \rho} \\ \frac{\partial L}{\partial M} = \epsilon - \frac{\partial U}{\partial t} + \frac{P}{\rho^2}\frac{\partial \rho}{\partial t} \\ \frac{\partial X_i}{\partial t} = -\frac{\partial F_i}{\partial M} + \Psi_i,\ 1 \le i \le n_{\rm X} \end{cases} \tag{1}$$

are recalled for notation and reference. Standard symbols are employed; t: time, G: gravitational constant, $\Omega(M,t)$: angular velocity, $\nabla \equiv \partial \ln T / \partial \ln P$: temperature gradient, $L(M,t)$: luminosity, ϵ: rate of nuclear energy release, U: internal energy per unit of mass, $X_i(M,t)$: fraction of unit mass which consists of nuclei of type i, $\mathcal{X} \equiv (X_1, \ldots, X_{n_{\rm X}})^T$, $F_i(M,t)$: flow of X_i due to diffusion, Ψ_i: creation rate of X_i due to thermonuclear reactions, $n_{\rm X}$: number of chemical species.

2.2. Diffusion of chemicals

For the chemical species $i = 1, \ldots, n_X$, in its most general form, the flow $F_i(M,t)$ is written:

$$F_i = -4\pi R^2 \rho \left(4\pi R^2 \rho D_i \bullet \nabla_{\rm M}\mathcal{X} - v_i X_i\right), \tag{2}$$

the components $d_{i,j},\ i \neq j$, of the vector:

$$D_i(M,t) \equiv (d_{i,1}, \ldots, d_{i,n_X})^T,$$

are the coefficients, $d^\star_{i,j}$, of microscopic atomic diffusion for the chemical species $\#i$ with respect to the species $\#j$; the (i,i)-th component:

$$d_{i,i} \equiv d^\star_{i,i} + d_{\rm T} \tag{3}$$

also includes the turbulent diffusion $d_{\rm T}$; $v_i(M,t)$ is the velocity of diffusion; the "$\bullet$" denotes the inner product:

$$D_i \bullet \nabla_{\rm M}\mathcal{X} \equiv \sum_j d_{i,j}\frac{\partial X_j}{\partial M}.$$

Recall that, owing to diffusion, the chemical composition is a continuous function.

Extended vector of chemicals. With the diffusion of Z, the content of heavy elements per unit of mass, and/or of $\mathcal{M}_\Omega \equiv \Omega R^2$, the angular momentum per unit of mass, it is convenient to generalize the vector of chemicals by adding one/two components, since, with *ad hoc* coefficients, it fulfills a diffusion equation similar to Eq. (3). Hereafter, otherwise stated, for sake of simplicity, the previous notations, i.e?, $\mathcal{X}$ and n_X, will be also used, respectively, for the extended vector of chemicals and for its length:

$$\mathcal{X} = \mathcal{X}(M,t) \equiv (X_1, \ldots, X_{n_{\rm X}}, Z, \mathcal{M}_\Omega)^T.$$

[2] Recall that, due to the mixing of chemicals a discontinuity may occur in the density profile at the limit of convective cores.

2.3. Convection

At each level, according to a choice made a priori, either the Schwarzchild's or the Ledoux's criterion allows to decide if the energy transport is made by radiation or by convection.

2.3.1. Mixing

In convective zones, contingently extended by overshooting (hereafter named "Mixed Zones", MZ), the characteristic time scale of the convection is small with respect to the thermonuclear time scales, then the MZ are *quasi instantaneously* mixed and their chemical composition is homogeneous. Owing to thermonuclear reactions, at each Limit between a Mixed zone and a Radiative zone (LMR), the chemical composition may have discontinuity. It is emphasized that, if it is not regenerated, a long-lasting discontinuity on chemicals is an unphysical situation. With CESAM, the mixing is made either by standard integration, i.e., instantaneous mixing, or by diffusion.

Instantaneous mixing. For a given MZ, let F_i^+ and F_i^- be the flows of X_i at each LMR, the last equation of the system Eq. (1) becomes (Clayton, Sect. 6.3, 1968):

$$\frac{\mathrm{d}\bar{X}_i}{\mathrm{d}t} = \frac{F_i^+ + \int_{\mathrm{MZ}} \Psi_i(P,T,\bar{\mathcal{X}},t)\mathrm{d}M + F_i^-}{\int_{\mathrm{MZ}} \mathrm{d}M} \tag{4}$$

where each component $\bar{X}_i$ of $\bar{\mathcal{X}}$, the vector of the mean abundances, is expressed as:

$$\bar{X}_i = \int_{MZ} X_i \mathrm{d}M \;/\; \int_{MZ} \mathrm{d}M.$$

The reaction rates, $\Psi_i(P,T,\mathcal{X},t)$, are non-linear functions of the abundances, therefore, at any point M of a MZ, the rate Ψ_i has to be calculated with $\bar{\mathcal{X}}$ the *mean values, at time t,* of the abundances over the MZ; hence the calculation of the chemical composition is an integro-differential problem.

Mixing by diffusion. As suggested by Eggleton (1971, 1972), the convective mixing can be modelled by *turbulent* diffusion; that can be made by adding a "mixing" diffusion coefficient $d_{\mathrm{M}}(M,t)$ to the turbulent diffusion d_{T}; Eq. (3) becomes:

$$d_{i,i} \equiv d^{\star}_{i,i} + d_{\mathrm{T}} + d_{\mathrm{M}}. \tag{5}$$

Mixing of angular momentum. In MZ solid rotation is assumed, there, the angular velocity is written:

$$\Omega(m,t) = \frac{\int_{\mathrm{MZ}(t)} r^2(m,t-\Delta t)\Omega(m,t-\Delta t)\mathrm{d}m}{\int_{\mathrm{MZ}(t)} r^2(m,t)\mathrm{d}m}.$$

with the integrals taken over all the MZ at time t; Δt is the time step. Likewise, when the diffusion of the angular momentum is taken into account, $\mathcal{M}_\Omega$ is homogenized, in each MZ, by strong turbulent diffusion.

2.3.2. Overshooting, undershooting

At LMR the velocity of convective eddies is not zero, therefore the convective motions can penetrate into the radiative zone. Owing to the small characteristic time scale of the convection, the matter is homogenized within the overshoot/undershoot zone; if, there, the temperature gradient keeps its convective adiabatic value with a discontinuity at the limit of the extension, one speaks of "convective penetration" (Zahn 1991).

2.4. Boundary conditions

With respect to the independent variables (M,t), boundary and initial conditions for the dependent variables P, T, R and L must be specified.

2.4.1. Mass loss and mass change

Let $\dot{M} \leq 0$ be the rate of external mass loss due to stellar wind and $\dot{\mathcal{M}} \leq 0$ be the change of mass due to mass defect (for the Sun $\dot{\mathcal{M}} \simeq L/\mathcal{C}^2 \sim 10^{-14} M_\odot\ y^{-1} \sim \dot{M}$):

$$\dot{\mathcal{M}}(t) = \int_0^{M_\star(t)} \frac{\epsilon + \epsilon_\nu}{\mathcal{C}^2} \mathrm{d}m$$

ϵ_ν is the energy of neutrinos, $\mathcal{C}$ the velocity of light and $M_\star(t)$ the total mass of the star at time t:

$$M_\star(t) = M_{\mathrm{ini}} + \int_0^t \left(\dot{M}(x) + \dot{\mathcal{M}}(x)\right) \mathrm{d}x$$

with M_{ini} as the initial mass of the star. It is assumed that the mass lost by stellar wind is simply detached from the star by some process which is not described.

Loss of angular momentum. Likewise, per unit of time, the amount of angular momentum lost, caused only by mass loss, amounts to:

$$\dot{\mathcal{M}}(t)_\Omega = \dot{M}(t)\Omega(M_\star,t)R_{\mathrm{A}}^2(t),$$

with R_{A} as the Alfèn radius, where matter decouples from the magnetic field (Schatzman 1959).

2.4.2. Boundary conditions at center

Due to the hypothesis of spherical symmetry, the radius, luminosity and the fluxes of chemical and of angular momentum vanish at the center, i.e., at $M \equiv 0$:

$$R(0,t) = 0,\ L(0,t) = 0, \tag{6}$$

and:

$$F_i(0,t) = 0,\ i = 1,\ldots,n_{\mathrm{X}},\ F_\Omega(0,t) = 0. \tag{7}$$

2.4.3. External boundary conditions

The problem of the external boundary conditions is more intricate. Inside a star, in the optically thick medium, the radiative flux can be derived from the diffusion equation which is the limit of the transfer equation for large optical depth (Mihalas 1978, Sect. 2.5). Since it is beyond our possibilities to include a full atmosphere calculation into a whole stellar model, one separates the internal structure calculations where the diffusion approximation is valid, from an outer part where the atmosphere calculation is made under simplified assumptions; in that sense the atmosphere is only "reconstituted". The limit between the two parts, where the bottom of the atmosphere coincides with the top of the envelope, must be located at a Rosseland optical depth $\tau_{\rm b}$ large enough for the diffusion approximation to be valid. Precise radiative transfer calculations (Morel et al. 1993, 1994) have shown that $\tau_{\rm b} \geq 20$ if one needs to be sure that the diffusion approximation strictly satisfied at all wavelengths; therefore, owing to convection, the use of purely radiative $\mathcal{T}(\tau)$ laws, such as Eddington's law (Maeder & Meynet 1987), are not valid for stars of mass $M_\star \lesssim 1.8\ M_\odot$ which have always a significant external convective zone.

At time t, the bottom of the atmosphere is connected at the outermost boundary of the envelope by three functions of luminosity, radius and time: pressure $P_{\rm b}(R,L,t)$, temperature $T_{\rm b}(R,L,t)$ and mass $M_{\rm b}(R,L,t)$. These three functions are provided by the reconstitution of the atmosphere. At any point in the atmosphere, the chemical composition is assumed to be the chemical composition of the outer layer of the envelope. It is emphasized that the differential problem Eq. (1) has, then, an external *open limit*, since $M_{\rm b}$ changes with time though it remains very close to the total mass of the star, $M_\star(t)$, typically $M_\star(t) - M_{\rm b}(R,L,t) \sim 10^{-10} M_\star(t)$; a very elegant solution to the numerical problem of the open limit is obtained via the automatic location of grid points as seen Sect. 3.2.2.

Simplified external boundary conditions. For some applications only an estimate of the radiative energy transfer in the outer layers is sufficient and good results are obtained with the single shell approximation as described by Christensen-Dalsgaard (1988). Working with the equation of hydrostatic equilibrium, the definition of the Rosseland optical depth, $\mathrm{d}\tau = -\kappa\rho \mathrm{d}R$ with κ as the Rosseland mean opacity, setting the definition of the effective temperature $T_{\rm eff}$ as $T_{\rm b}$, the simplified external boundary conditions are written:

$$\begin{aligned} &\frac{\mathrm{d}P}{\mathrm{d}\tau} = \frac{GM_{\rm b}}{\kappa_{\rm b} R_{\rm b}^2} - \frac{2\Omega^2 R_{\rm b}}{3\kappa} \sim \frac{P_{\rm ext} - P_{\rm b}}{\tau_{\rm ext} - \tau_{\rm b}} = \frac{P_{\rm b}}{2/3}, \\ &T_{\rm b} = T_{\rm eff} = 4\pi\sigma R_{\rm b}^2 L_{\rm b}, \end{aligned} \tag{8}$$

here it is assumed that the pressure cancels, $P_{\rm ext} = 0$, at the optical depth, $\tau_{\rm ext} = 0$, of the outer limit of the atmosphere, likewise the optical depth of the bottom of the atmosphere is assumed to be $\tau_{\rm b} = 2/3$; σ is the Stefan-Boltzman constant. The mass $M_\star$, the radius $R_\star$ and the luminosity $L_\star$ of the star respectively then is written:

$$M_\star = M_{\rm b},\ R_\star = R_{\rm b},\ L_\star = L_{\rm b}. \tag{9}$$

The unknown, $P_{\rm b}(t)$, $T_{\rm b}(t)$ and $M_{\rm b}(t)$ are solutions of the non-linear set of Eq. (8), owing to the conditions Eq. (9).

Precise external boundary conditions. For other applications, as for helioseismology purposes, since the eigenmodes are reflected in the atmosphere, for each level, one needs accurate values of the physical quantities of necessity for the calculation of the frequencies, i.e., a detailed "reconstitution" of the atmosphere is required; a standard technique is the use of a so-called $\mathcal{T}(\tau, T_{\rm eff}, g)$ law (Henyey et al 1959; Kippenhahn et al. 1968); here, as far as the atmosphere has a small extent, the gravity g is constant within and equal to the total gravity of the star, $g_\star \equiv GM_\star/R_\star^2$.

A difficulty with the detailed reconstitution of the atmosphere is connected to the location of the stellar radius $R_\star$ which encloses the mass of the star $M_\star$; using the standard definition (Schatzman & Praderie 1990), at time t, the radius of the star is defined at the level of optical depth $\tau_\star$ where the temperature is equal to the effective temperature:

$$\mathcal{T}(\tau_\star, T_{\rm eff}, g_\star) = T_{\rm eff} = \sqrt[4]{\frac{L_\star}{4\pi\sigma R_\star^2}}. \tag{10}$$

According to model atmospheres calculated with the Kurucz's ATLAS9 code (Kurucz, 1991), for a $1\ M_\odot$ model, from Pre-Main Sequence (PMS) initial conditions to present age, $\tau_\star$ varies within the interval $\sim [2/5,\ 2/3]$, since $T_{\rm eff}$ and $g_\star$ vary. In some cases, e.g. along the evolution of the Sun from the ZAMS to present time, the changes of $\tau_\star$ remain small and can be neglected, but it is not the case if PMS or post main-sequence are involved – see Morel et al. (1994), for a more complete discussion.

With a time dependent stellar radius, the set of differential equations to be solved for the reconstitution of the atmosphere is written:

$$\begin{cases} \frac{\mathrm{d}P}{\mathrm{d}\tau} = \frac{GM}{\kappa R^2} - \frac{2\Omega^2 R}{3\kappa} \\ \frac{\mathrm{d}R}{\mathrm{d}\tau} = -1\ /\ \kappa\rho \\ \frac{\mathrm{d}M}{\mathrm{d}\tau} = -4\pi R^2\ /\ \kappa \\ \frac{\mathrm{d}R_\star}{\mathrm{d}\tau} = 0 \\ \frac{\mathrm{d}\tau_\star}{\mathrm{d}\tau} = 0 \end{cases} \quad \begin{cases} \text{boundary conditions} \\ \rho(\tau_{\rm min}) = \rho_{\rm ext} \\ M(\tau_\star) = M_\star \\ R(\tau_\star) = R_\star \\ T_{\rm eff} = \mathcal{T}(\tau_\star, T_{\rm eff}, g) \\ R(\tau_{\rm b}) = R_{\rm b}. \end{cases} \tag{11}$$

Following the standard method (Stoer & Bulirsch 1973, Sect. 7.3.0), the two last differential equations have been added for solving the differential problem with the open inner boundary at $\tau = \tau_\star$; they allow to link $R_\star$ and $\tau_\star$

to the other unknowns. At the optically thin limit of the atmosphere, defined by $\tau = \tau_{\rm min}$, the density has the value $\rho_{\rm ext}$ given by the model atmosphere; here one assumes $\tau_{\rm min} \equiv 10^{-4}$, that roughly corresponds to the optical depth of the temperature minimum of the Sun photosphere; hence the model does not include the non LTE outerparts of the atmosphere where the density and temperature values take place outside of the ranges of the standard opacity and EOS tables. Boundary conditions are therefore located at three different levels: $\tau = \tau_{\rm b}$, $\tau = \tau_\star(t)$ and $\tau = \tau_{\rm min}$; indeed, $\rho_{\rm ext}$ is a function of time since $\rho_{\rm ext}(g_\star(t))$. At time t, the solution of Eq. (11) gives $P_{\rm b}$, $T_{\rm b}$ and $M_{\rm b}$ for given $R_{\rm b}$ and $L_{\rm b}$.

Obviously, the $T(\tau)$ laws and the internal structure need to be computed with consistent physics (EOS, opacity, convection theory, mixing-length parameter, chemical composition etc...).

External boundary conditions for diffusion of chemicals. As far as the amount of material in the atmosphere remains negligible the changes of abundances caused by diffusion can be ignored and a homogeneous chemical composition can be assumed there. As already stated, the mass loss by mass lost and also the angular momentum lost, are here assumed simply detached by processes which are not described, at the level $M = M_{\rm b}(t)$, due to the mass conservation, there is no input nor output of chemicals and angular momentum therefore:

$$F_i(M_{\rm b}(t), t) = 0,\ i = 1, \ldots, n_{\rm X}. \tag{12}$$

2.5. Initial conditions

At time $t \equiv 0$, one has to specify the values of pressure, $P(M, 0)$, temperature $T(M, 0)$, radius $R(M, 0)$, luminosity $L(M, 0)$ and vector of chemical $\mathcal{X}(M, 0)$, at any location within the star interior, $M \in [0, M_{\rm b}(t = 0)]$; they are derived from an homogeneous stellar model of, either, PMS, or, Zero Age Main-Sequence (ZAMS).

2.5.1. PMS initial models

Along the PMS evolution the radiative losses are only sustained by the release of gravothermal energy; as the chemicals have no time dependence (Reiter et al. 1995), the gravothermal energy is proportional to the partial derivative of the entropy with respect to time:

$$\epsilon_{\rm G} \sim -T \frac{\partial S}{\partial t}.$$

As a consequence, for a zero age PMS model, though in quasi-hydrostatic equilibrium, the gravothermal energy cannot be taken as 0, as it does for ZAMS models. At the onset of the quasi-static PMS phase, i.e., at the beginning of the Hayashi line (Kippenhahn & Weigert 1991), the stars are fully convective except, perhaps, in a small outer region (Iben 1975); the entropy is then constant within the star, therefore the equation of energy can be written:

$$\frac{\partial L}{\partial M} = \epsilon_{\rm G} \sim -T \frac{\partial S}{\partial t} = cT$$

here $c(t)$ is the so-called contraction factor; it characterizes the fully convective model in quasi-static equilibrium; for stars with the empirical value $c = 0.02\ L_\odot\ M_\odot^{-1}\ {\rm K}^{-1}$ the starting point of PMS evolution is located in the upper right corner of the HR diagram; it can be adjusted to its requested place just by changing c.

For a given star, let an initial PMS model # 1 be characterized by a contraction factor c_1 and a model # 2 with c_2 ($c_2 \neq c_1$); between models 1 and 2, the change of gravitational energy is equal to the radiative losses during the time step, Δt, which, approximatively, amounts to:

$$\Delta t \sim 2\ GM^2 \frac{|R_1 - R_2|}{(L_1 + L_2) R_1 R_2}. \tag{13}$$

Therefore Eq. (13) gives an approximate value for the evolutionary time scale Δt of the model characterized by the contraction factor $c \simeq (c_1 + c_2)/2$; typically one uses: $c_2 \sim 1.1\ c_1$.

Transitions between pre main-sequence, main-sequence and post main-sequence. It is assumed that a PMS model becomes a main-sequence model as soon as 99% of the energy generated has a nuclear origin; at that time, the model is chemically inhomogeneous, in opposition ZAMS models are homogeneous. Likewise, as soon as, at center, the abundance of $^1{\rm H} \leq 10^{-5}$ a main-sequence model becomes a POST main-sequence model.

2.5.2. ZAMS initial models

ZAMS models are homogeneous and in hydrostatic equilibrium, i.e., they fulfill the equations Eq. (1) with the gravothermal term equal to zero and homogeneous chemical composition. A ZAMS model is not a physical situation because, during the interval of time elapsed from the instant of the ignition of the thermonuclear reactions which occurs when the central temperature reaches $T_{\rm c} \sim 10^6$ K, to the instant when physical conditions similar to the ZAMS are established – i.e., when $T_{\rm c} \sim 15\,10^6$ K, for 1 $M_\odot$ – the chemicals was not processed by amounts corresponding to the values of density and temperature (it has been found (Rossignol 1995) that, everything else fixed, for ages larger than $\gtrsim$ 150 My, the internal structures of a solar model evolved from ZAMS and of a solar model evolved from PMS but older by $\sim$ 30 My, are very similar).

3. Solving the two-point boundary initial value problem

The equations of stellar structure, Eq. (1), and their numerical counterpart, Eq. (21), are non-linear; in CESAM

they are solved using the so-called *damped Newton-Raphson* method, which differs from the standard relaxation method (Clayton 1968, Sect. 6.4) by the fact that the change in the unknowns are reduced; that allows to follow the "good descent direction" given by the jacobian of the linearized equations (Conte & de Boor 1987, Sect. 5.2) of the non-linear problem solved as an optimization problem; doing that the time step remains of reasonable size, even with shell sources.

3.1. Overview on numerical integration

With instantaneous mixing, the set of partial differential equation Eq. (1) is an initial boundary value, integro-differential problem[3]; for the numerical solution, following Henyey et al. (1959), it is split into two differential problems:

1. The "evolution of chemicals" in this first step, the chemical composition is updated for the time step Δt, taking into account the mixing in MZ; in this first step, only $\mathcal{X}$ changes, the other variables, i.e., P, T, R, L, remain fixed.
2. The "quasi-static equilibrium", in this second step, the dependent variables, i.e., pressure, temperature, radius and luminosity, are adjusted to fulfill the quasi-static equilibrium with the value of the chemical composition, $\mathcal{X}$, previously updated.

For each time step Δt, starting from an approximate solution, the two problems are solved sequentially until global convergence; the whole process is fully implicit; *all* the variables P, T, R, L, $\mathcal{X}$ are centered at time t (Bressan et al. 1993 center the chemical composition at half time step, that save computing effort but can generate instabilities in case of stiffness).

3.2. Numerical solution of the "quasi-static equilibrium"

The numerical solution of the quasi-static equilibrium is made using the B-spline collocation method described in Appendix C5; the basic idea is to seek the unknown functions as piecewise polynomials which are, by turn, projected on their B-spline basis of order $h_{\rm q}$ (i.e., of degree $h_{\rm q}-1$), therefore the (non-linear) discretized differential equations only involve the projections and are solved for them; finally, their knowledge allows to rebuilt the solution, i.e., the piecewise polynomials, for any location.

3.2.1. The lagrangian variables employed

With the mass as the independent variable, the three first equations of the differential system Eq. (1) have a singularity at center, $M \equiv 0$; to overcome the difficulty, Taylor series have been employed (Kippenhahn et al. 1968; Paczynski 1969). Here an alternate approach is applied: first, variables which avoid the central singularities are employed and, second, the equations are not written right at center, as quoted Appendix C5; therefore, for the first shell, there is no need of a peculiar algorithm. Owing to the exponents 2/3 and 2 which are optimal (see Appendix C1), among all sets of variables which avoid the central singularities, the Eggleton (1971) variables[4]:

$$\left(\frac{M}{M_\odot}\right)^{\frac{2}{3}},\ \left(\frac{R}{R_\odot}\right)^{2},\ \left(\frac{L}{L_\odot}\right)^{\frac{2}{3}}, \tag{14}$$

$L \geq 0$, lead to the most precise numerical solution. From the surface to the center, the pressure and the temperature typically change, respectively, by eighteen and five orders of magnitude, therefore logarithms are used for those variables. *In fine,* the following set of lagrangian variables, free from central singularities, is employed:

$$\begin{array}{l} \xi = \ln P,\ \eta = \ln T, \\ \mu = \left(\frac{M}{M_\odot}\right)^{\frac{2}{3}}, \zeta = \left(\frac{R}{R_\odot}\right)^{2},\ \lambda = \left(\frac{L}{L_\odot}\right)^{\frac{2}{3}}. \end{array} \tag{15}$$

3.2.2. Automatic location of grid points

Due to large gradients the density of mesh points cannot be kept constant along the model; moreover, in the course of an evolution, the areas affected by large gradients change, therefore the grid cannot kept fixed. The most usual method for grid refinement consists by adding or subtracting points according to criterions (see, for example, Henyey et al. 1959; Kippenhahn et al. 1968). Though this method is very simple in its principle, in practice, it is difficult to be properly implemented; an automatic mesh refinement is more convenient. Here, at a given time t, the number $n(t)$ of mesh points is given and their locations are fixed by fulfilling the condition that, from one grid point to the next, the jump of a *strictly monotonous* "distribution function", $Q(\mu, t)$, is equal to a "distribution constant" $C(t)$ (Eggleton 1971; Press et al. 1986, Sect. 16.5); at each time t the distribution of the grid points, $\mu_i, i = 1, \ldots, n$, therefore satisfies:

$$Q(\mu_{i+1}, t) - Q(\mu_i, t) \equiv C(t), \quad i = 1, \ldots, n-1. \tag{16}$$

The choice of $Q(\mu, t)$ is based on an a priori knowledge of the behavior of the solution. For each value t of the time, one defines an "index" function $q(\mu, t)$ mapping $[1, \mu_{\rm b}]$ on $[1, n]$; the shell with the index 1 (respt. n) corresponds to the center (respt. to the top of the envelope). Therefore the integration is made on an *equidistant grid*. In terms of the derivative of Q with respect to q:

$$\psi(t) \equiv \left(\frac{\partial Q}{\partial q}\right)_t, \tag{17}$$

[3] Formally, with diffusion and turbulent mixing, the integro-differential character disappears, the problem is only differential.

[4] If negative values of luminosity are expected, the eulerian set of variables given Sect. 3.2.6, ought to be employed.

Eq. (16) becomes:

$$\left(\frac{\partial\psi}{\partial q}\right)_t = 0. \tag{18}$$

Note that Q is a linear function of q as soon as the Eqs. (17) and (18) are fulfilled. The change of variables $\mu \to q(\mu, t)$ gives:

$$\psi(t) = \theta \left(\frac{\partial\mu}{\partial q}\right)_t,$$

where:

$$\theta(\mu, t) \equiv \left(\frac{\partial Q}{\partial \mu}\right)_t, \tag{19}$$

can be derived from the analytic form of $Q(\mu, t)$. Thus, there are two more unknowns: $\psi(t)$ and $\mu(q, t)$; they fulfill a system of differential equations of first order with boundary conditions:

$$\left(\frac{\partial\mu}{\partial q}\right)_t = \frac{\psi}{\theta},\ \left(\frac{\partial\psi}{\partial q}\right)_t = 0,\ \text{with}\ \begin{cases} q = 1,\ \mu = 0 \\ q = n,\ \mu = \mu_{\rm b}, \end{cases} \tag{20}$$

here $\mu_{\rm b}$ is computed by Eq. (15) with the value of $M_{\rm b}$ obtained at the bottom of the atmosphere. The set of equations to be solved on the *equidistant* grid, $q_i \equiv i$, $i = 1, \ldots, n$ is therefore:

$$\begin{cases} \frac{\partial\xi}{\partial q} = \left[-\frac{3G}{8\pi}\left(\frac{M_\odot}{R_\odot^2}\right)^2\left(\frac{\mu}{\zeta}\right)^2 + \frac{M_\odot}{4\pi R_\odot}\sqrt{\frac{\mu}{\zeta}}\Omega^2\right]\frac{{\rm e}^{-\xi}\psi}{\theta} \\ \frac{\partial\eta}{\partial q} = \frac{\partial\xi}{\partial q}\nabla \\ \frac{\partial\zeta}{\partial q} = \frac{3}{4\pi}\frac{M_\odot}{R_\odot^3}\frac{1}{\rho}\sqrt{\frac{\mu}{\zeta}}\frac{\psi}{\theta} \\ \frac{\partial\lambda}{\partial q} = \frac{M_\odot}{L_\odot}\sqrt{\frac{\mu}{\lambda}}\left[\epsilon - \left(\frac{\partial U}{\partial t}\right)_{\mu_{\rm d}} + \frac{\exp\xi}{\rho^2}\left(\frac{\partial\rho}{\partial t}\right)_{\mu_{\rm d}}\right]\frac{\psi}{\theta} \\ \frac{\partial\mu}{\partial q} = \frac{\psi}{\theta} \\ \frac{\partial\psi}{\partial q} = 0. \end{cases} \tag{21}$$

The initial and boundary conditions are straightforwardly expressed in terms of q. Note that the derivative, with respect to time, of the specific internal energy and of the density should be taken along directions ${\rm d}M_{\rm d} = 0$, i.e., ${\rm d}\mu_{\rm d} = 0$, taking into account the change of mass due to the mass defect. Indeed, the solution, by the damped Newton Raphson scheme, of the non-linear Eq. (21), necessitates the knowledge of the derivatives of ρ, ϵ and U, with respect to the mass, taking into account the changes of chemical composition; that is the more restrictive conditions imposed by the use of this automatic allotment of mesh points; it is also a consequence of the fact that the integro-differential problem, Eq. (1), cannot be solved as a whole since, along the evolution, convective zones appear, disappear, cede or recede with not fixed limits. Moreover with an equidistant mesh in q, differences between close numbers are avoided; that is particularly sensitive in the external part of the envelope where the changes of mass between two adjacent grid points are very small.

Choice of Q. Q should be a strictly monotonous, two times differentiable, function, and as simple as possible. By experiments, it has been found[5] that:

$$Q = \Delta_\xi \xi + \Delta_\mu \mu \tag{22}$$

is, in all, the most convenient form; for the two "distribution factors" Δ_ξ and Δ_μ, the *heuristic* values:

$$\Delta_\xi \equiv -1,\ \Delta_\mu \equiv 15,$$

are close to those used by Eggleton (1971). The function $\theta(\mu, t)$ can now be explicitly calculated using Eq. (19) and Eq. (21). In the core, the pressure gradient is not large and the mesh refinement is monitored by the changes of μ, i.e., the mass; while, in the outermost part of the envelope the repartition function is controlled by the changes of ξ, i.e., the pressure, due to its large gradient; there, from a grid point to the next, the mass changes are very small, typically $\sim \Delta M \gtrsim 10^{-10} M_\odot$, even $\sim \Delta M \gtrsim 10^{-12} M_\odot$, while for, the pressure, the changes are of the order of $\sim 10\%$ (with $C(t) \sim 0.1$, see next paragraph); a similar situation occurs on the neighborhood of shell sources.

Optimization of the number of grid points. Between a PMS initial model and an evolved model at the beginning of the ^{4}He burning, the central pressure is magnified by more than 30, that also affects the distribution constant $C(t)$; the accuracy is ensured whatever the age is, if the repartition constant, is kept almost fixed with respect to time; that is done by increasing (or decreasing) the total number of shells in such a way that $C(t)$ remains within $\pm 2\%$, of its initial value. With $C(t) \simeq 0.1$, $\Delta_\xi = -1$ and $\Delta_\mu = 15$, the relative change in pressure within a shell is typically 10% and the number of zones in a PMS initial solar model is of the order of 250, it increases to ~ 450 at present solar age and more than ~ 800 at the onset of the helium flash.

Setting a grid point on a LMR. The algorithm of automatic location of grid points has been extended in order to shift automatically a grid point in a close vicinity of each LMR; the method is described in Appendix B2.

3.2.3. Boundary conditions at center

With respect to the independent variable q, the center corresponds to $q = 1$, the three inner boundary conditions are simply written:

$$\zeta(1, t) = 0,\ \lambda(1, t) = 0,\ \mu(1, t) = 0.$$

[5] For models of interiors of giant planets (Guillot & Morel 1995) another form for Q is used.

3.2.4. External boundary conditions

As seen in Sect. 2.4.3, at time t, the bottom of the atmosphere is connected at the outermost boundary of the envelope by the three functions: pressure $P_{\rm b}(R,L,t)$, temperature $T_{\rm b}(R,L,t)$ and mass $M_{\rm b}(R,L,t)$ of the radius, luminosity and time; they are derived from the outer boundary conditions through a reconstitution of the atmosphere. With the variables of Eq. (15), at $q=n$, the external boundary conditions for the envelope are written:

$$\begin{array}{l}\xi(n,t)-\xi_{\rm b}(\zeta_{\rm b},\lambda_{\rm b},t)=0\\ \eta(n,t)-\eta_{\rm b}(\zeta_{\rm b},\lambda_{\rm b},t)=0\\ \mu(n,t)-\mu_{\rm b}(\zeta_{\rm b},\lambda_{\rm b},t)=0\end{array} \qquad (23)$$

where $\xi_{\rm b}$, $\eta_{\rm b}$ and $\mu_{\rm b}$ are the values, at time t of, respectively, ξ, η and μ at the bottom of the atmosphere, of radius $R_{\rm b}=\sqrt{\zeta_{\rm b}}R_\odot$ and luminosity $L_{\rm b}=\sqrt{\lambda_{\rm b}^3}L_\odot$, where the diffusion approximation becomes valid. Hence the grid adjustment solves trivially the problem of the open limit.

Simplified external boundary conditions. In that case, $M_{\rm b}\equiv M_\star$ and $\mu_{\rm b}\equiv 1$; $P_{\rm b}$ and $T_{\rm b}$, are derived from Eq. (8) with $R_\star\equiv R_{\rm b}=R_\odot\sqrt{\zeta(n,t)}$ and $L_\star\equiv L_{\rm b}=L_\odot\sqrt{\lambda^3(n,t)}$. The Rosseland mean opacity κ is a function of density and temperature, therefore the non-linear system of Eq. (23) must be solved by iterations for $\xi_{\rm b}$, $\eta_{\rm b}$, $\mu_{\rm b}$ and for their derivatives with respect to ζ and λ.

Precise external boundary conditions. As described in Sect. 2.4.3, the precise reconstitution of an atmosphere consists in a differential problem, with boundary conditions at three different levels: $\tau_b\gtrapprox 10$, $\tau_{\rm min}\lessapprox 10^{-4}$ and $0.3\lessapprox\tau_\star\lessapprox 0.6$; recall that, at $\tau=\tau_\star(t)$, defined by Eq. (10), there is a *open* inner limit; the solution given to this numerical challenge is described in Appendix B3.

3.2.5. Gravothermal energy

The gravothermal energy is written[6]:

$$-\epsilon_{\rm G}=\frac{\partial U}{\partial t}-\frac{P}{\rho^2}\frac{\partial\rho}{\partial t}. \qquad (24)$$

For stability purposes, at each collocation point, $\epsilon_{\rm G}$ is discretized by the backward difference formula of first order:

$$-\epsilon_{\rm G}=\frac{U^{t+\Delta t}-U^t}{\Delta t}-\frac{P}{\rho^2}\frac{\rho^{t+\Delta t}-\rho^t}{\Delta t}+O(\Delta t^2). \qquad (25)$$

The use of this low order formula is justified by the fact that the entropy variations are negligible on the main-sequence, otherwise the models are so complicated that high order schemes can lead to instabilities and therefore are not recommended. In the plane $(M\times t)$, Eq. (24) must be written along directions of constant mass, i.e., including the mass defects, ${\rm d}M_{\rm d}=0$ or ${\rm d}\mu_{\rm d}=0$; at time t, density and specific internal energy are derived, via EOS, from pressure, temperature and chemical composition (see Sect. 3.3.1) obtained through the *non-linear* inverse interpolation scheme "$\hookrightarrow$":

$$M_{\rm d}\rightarrow\mu_{\rm d}\rightarrow\begin{cases}\hookrightarrow q\ \rightarrow(\xi,\eta)\rightarrow(P,T),\\ \rightarrow\nu\ \rightarrow\mathcal{X},\end{cases}$$

with $\nu\equiv(M/M_\odot)^{2/3}$ (see Sect. 3.3.1).

3.2.6. An eulerian set of variables

Note that, with (R,t) as an eulerian independent variable, Eq. (1) have no singularity but, as the stellar radius varies with respect to time, the external limit, at $M=M_{\rm b}$, is an open limit; though that is not a difficulty for the numerical method of integration used – see Sect. 3.2.2 –, the lagrangian set of variables Eq. (15), is preferred owing to its highest numerical accuracy as demonstrated Appendix B1. With the exponent 2/3 for λ, in Eq. (15), the luminosity must remain non-negative, i.e., $\lambda\geq 0$; otherwise, though less accurate, the following set of eulerian variables ought to be employed:

$$\xi=\ln P,\ \eta=\ln T,\ \mu=\tfrac{M}{M_\odot},\ \zeta=\tfrac{R}{R_\odot},\ \lambda=\tfrac{L}{L_\odot}. \qquad (26)$$

Similarly, for the eulerian variables, one defines: $\psi(t)=\left(\frac{\partial Q}{\partial q}\right)_\zeta$ and $\theta(\zeta,t)=\left(\frac{\partial Q}{\partial\zeta}\right)_t$. Equations, initial and boundary conditions are straightforwardly derived.

3.3. Numerical solution of the "evolution of chemicals"

To be consistent it is desirable to be able to solve, with algorithms of same orders, the two differential problems, i.e., the "quasi-static equilibrium" and the "evolution of chemicals". One needs also a suitable monitoring of the time step derived, if possible, from an estimate of the accuracy of the integration.

3.3.1. Interpolation of chemicals

Due to the change of mass caused by the mass defect and mass loss, the chemicals need to be known at any point in the star. Here, with the spline-collocation method employed for the numerical integration of the quasi-static equilibrium, the collocation points, where the discretized differential equation are fulfilled, differ from the grid points; moreover, due to the grid adjustment, the collocation points have not fixed values in mass; therefore an interpolation algorithm is needed for the knowledge of the chemical composition at any point of the interval $[0,M_\star(t)]$. In fact, interpolation is needed as far as

[6] As pointed out by Strittmatter et al. (1970), Reiter et al. (1995), this formulation is correct while, in Eq. (4.27) of Kippenhahn & Weigert (1991), the changes of chemicals are ignored.

grid points are moved or added during the evolution; on the other hand, interpolations create numerical diffusion which, in some extent, stabilizes the numerical solution. The interpolation scheme needs to be, at least, as precise as the integration algorithm. Here one seeks the distribution of chemicals as piecewise polynomials on a lagrangian mesh. Due to the assumption of spherical symmetry, in the vicinity of the center the gradients of abundances are written:

$$\frac{\partial X_i}{\partial R} = O(R),\ i = 1, \ldots, n_{\rm X}.$$

Therefore

$$\frac{\partial X_i}{\partial M} = \frac{\partial X_i}{\partial R}\frac{\partial R}{\partial M} = O(R^{-1}),$$

with respect to the mass, the first derivative of the abundances have a singularity at the center so it cannot be interpolated accurately with respect to M using the variable such that $\nu \equiv (M/M_\odot)^{2/3}$:

$$\frac{\partial X_i}{\partial \nu} = \frac{\partial X_i}{\partial R}\frac{\partial R}{\partial \nu} = \frac{O(R)}{O(R)} = O(1),$$

the singularities are avoided. With diffusion (see Sect. 3.3.3), the solution of the diffusion equation agrees with the piecewise polynomial of interpolation; otherwise piecewise polynomial interpolation, with order $h_{\rm c}$, $2 \leq h_{\rm c} \leq 4$, with respect to ν is used (see Appendix C5). An *ad hoc* choice of the B-spline basis allows to take the discontinuities into account. Owing to its linearity, the interpolation scheme is conservative for any linear set of the unknowns – a proof is given in Appendix C4; therefore the total charge, total baryon number and baryon numbers involved in the PP and CNO cycles remain constant, within roundoff errors.

Due to (i) the splitting in two steps of the integration of the whole problem, and (ii) to the ability of restoring the solution at any point, a grid can be especially designed for the chemicals; this net is refined in the inner parts (recall that thermonuclear reaction rates have a high power law dependence with respect to the temperature) where the nuclear reactions are active.

Management of discontinuities. As noticed previously, a long-lasting discontinuity on chemical composition is an unphysical situation; therefore, when the diffusion is ignored, if no physical process is explicitly introduced, the discontinuities are smoothed by the numeric, the lower the order of the numerical scheme is, the more efficient is the smoothing. Satisfactory results have been obtained using, for a given time step, the mass points designed for the quasi-static problem, and for the next time step, mass points located at half distance between two neighbouring mass points designed for the quasi-static problem; ensuring, however, that the mass step, for the chemical composition is, at least, greater than $\Delta m \geq 5\,10^{-4}\ M_\odot$, except for each CZ where a minimum of 10 points is required. As far as a convective core increases, the chemicals undergo discontinuities at its limit, while, when it recedes, at any point localized in the zone between the previous and the new limits of the core, the values of abundances not only depend on the local temperature and density but, also, on how long that point has lasted in the mixed receding core; a similar situation occurs as soon as a MZ recedes from a radiative zone. Moreover in radiative zones, when the diffusion is ignored, though violating the physics, the discontinuities in chemicals *formally* stay so far they are not, again, embedded in a new extent of a convective zone. It is difficult to mimic in details and precisely all these tricky processes. In CESAM, the abundances at any point localized between the limit of a core and its location at the former time step, are obtained by linear interpolation, with respect to ν, between their values at the new and at the previous locations of the limit.

3.3.2. Standard evolution

In the radiative zones, without diffusion, the equations to be solved are written:

$$\frac{\partial X_{\rm i}}{\partial t} = \Psi_i,\ 1 \leq i \leq n_{\rm X}. \tag{27}$$

In MZ, the chemical composition is homogeneous and the equations for the mean abundances can be written (see Sect. 2.3.1):

$$\begin{aligned}\frac{{\rm d}\bar{X}_i}{{\rm d}t} &= \int_{\rm MZ} \Psi_i(P,T,\bar{\mathcal{X}},t){\rm d}M \Big/ \int_{\rm MZ} {\rm d}M \\ &= \int_{\rm MZ} \sqrt{\nu}\Psi_i(P,T,\bar{\mathcal{X}},t){\rm d}\nu \Big/ \int_{\rm MZ} \sqrt{\nu}{\rm d}\nu,\end{aligned} \tag{28}$$

therefore it is an integro-differential problem. Another numerical difficulty results from large ratios between the characteristic evolutionary time scales involved; they can be estimated by the ratio between the eigenvalues, $\lambda_{\rm min}$ and $\lambda_{\rm max}$, of minimum and maximum norms of the jacobian matrix:

$$J = \left(\frac{\partial \Psi_i}{\partial X_j}\right)_{i,\ j=1,\ldots,\ n_{\rm X}}.$$

Typically, with the physical conditions at the center of the present Sun, $T \sim 15\,10^6$ K, $\rho \sim 150$ g cm^{-3}, one has:

$$\frac{|\lambda_{\rm max}|}{|\lambda_{\rm min}|} \gtrsim 10^{18}.$$

Such differential problems are called "stiff" (Gear 1971; Hairer & Wanner 1991); special algorithms have been developed for their numerical solution; they ensure numerical stability even if the time step is larger than the smallest characteristic time scale. However, it is not possible to have accurate solution for all the variables, regardless of

the size of the time step; therefore, owing to the stability of the scheme, the numerical errors are damped out, a given accuracy being ensured for variables of interest. Furthermore, chemical abundances being positive numbers, oscillations around zero (as observed with the trapezoidal rule) are unsatisfactory. The so-called "L-stable" schemes (Hairer & Wanner, loc. cit.) have good stability properties without oscillations; they are suitable for the integration of the evolution of chemicals abundances. Equations (27) and (28) and their numerical counterparts are non-linear; they are also implicit, as the L-stable schemes are. The L-stable Implicit Runge Kutta (IRK) Lobatto IIIC formula with orders[7] p =1, 2 and 4 are available in CESAM; their coefficients are reproduced Table 5 (Appendix B4), $p = 1$ is the standard Euler's backward scheme (Hairer & Wanner, loc. cit.). For the Lobatto IIIC formulas with order p greater than two, values for the temperature and density are needed at intermediate time levels. They are estimated by interpolations of order four from successive models.

Stable integration with IRK formulas. Emphasis is made on the fact that, with stiff problems it is of great importance to use special algorithms specially designed for IRK formula; those used in CESAM are described in Appendix B4.

Numerical control of the accuracy. The comparison of solutions given by two IRK formula which differ by one order of accuracy, i.e., the so-called Fehlberg method (Stoer & Bulirsch 1979), allows an estimate $\varepsilon_{\rm e}$ of the numerical accuracy. Here the IRK formulas Radau IIA (Hairer & Wanner, loc. cit., Sect. IV.8) are used in connexion with Lobatto IIIC formulas. Let $\varepsilon_{\rm r}$ be the value required for the relative precision; an optimal value $\Delta t_{\rm opt}$ for the next time step is written:

$$\Delta t_{\rm opt} = \left(.9 \Delta t \frac{\varepsilon_{\rm r}}{\varepsilon_{\rm e}} \right)^{\frac{1}{1+p}} ,$$

here p is the order of the IRK formula. It has been observed that the robustness of the scheme is improved if only small changes for the time step are allowed for; therefore the estimate of the new time step $\Delta t_{\rm new}$ is taken as:

$$\Delta t_{\rm new} = \max \left(0.8 \Delta t, \min \left[1.2 \Delta t, \Delta t_{\rm opt} \right] \right) . \qquad (29)$$

This precise control of the numerical accuracy, practically, doubles the computing time; it is prohibitive in most cases, therefore the time step is simply adjusted in such a way that the changes of the abundances remain within fixed limits $\Delta_i,\ i = 1, \ldots, n_{\rm X}$.

[7] According to standard definitions the local error is O^{p+1}.

3.3.3. Evolution with diffusion

With diffusion, for every $\nu \in [0, \nu_{\rm b}]$ ($\nu_{\rm b} \equiv (M_{\rm b}/M_\odot)^{2/3}$), the set of equations to be solved is written:

$$\frac{\partial X_{\rm i}}{\partial t} = -\frac{\partial F_i}{\partial M} + \Psi_i = -\frac{2}{3\ M_\odot \sqrt{\nu}} \frac{\partial F_i}{\partial \nu} + \Psi_i, \qquad (30)$$

for $1 \leq i \leq n_{\rm X}$. As seen Sect. 2.3.1, the mixing in MZ is made by turbulent diffusion. Since Eq. (30) holds everywhere, the evolution of the chemical composition is no longer an integro-differential problem but a differential problem with boundary conditions given by Eq. (7) and Eq. (12); it is a mixed parabolic/hyperbolic problem. At each LMR, the abundances X_i and the fluxes F_i are continuous functions with discontinuous first derivatives owing to the jumps of $d_{\rm M}$ (see Sect. 2.3.1). The method of integration of the diffusion equation, written in finite-elements form, is described in Appendix B5.

Efficiency of the mixing by diffusion. Figure 1 plots, with respect to the mass fraction, the relative differences in sound velocity for two calibrated solar models calculated, respectively, with standard mixing and mixing by diffusion ($D^\star_{i,j} + D_{\rm T} = 0$, $D_{\rm M} = 10^{13}$ and $v_i = 0$, $\forall i, j$). The differences, at the level of 10^{-5}, show the similar efficiency of both approaches. Figure 2 plots, with respect to the radius fraction, the normalized abundances of ^{2}D, ^{3}He, ^{7}Li, ^{7}Be, ^{12}C at the onset of the main sequence for a non-standard solar model, evolved from PMS, including microscopic diffusion according to Michaud & Proffitt (1993); at that age (45 My) the convective core of the young Sun recedes, while the CZ is close to its present day location. One emphasizes on the well marked drop of the gradient of ^{2}D and on the smooth profile of ^{7}Li at the limit of the CZ; due to the mixing, in the convective core, the elements have a constant abundances except ^{8}Be since its nuclear time is of the order of the mixing time (∼100 days). As seen, the Petrov-Galerkin's solution is stable even with strong jumps of more than thirteen decades in the diffusion coefficients profiles.

4. General features for the implementation of the code

The flow chart of CESAM takes advantage of two spaces: a functional space (B-spline), where the differential equations are integrated with the mathematical formalism and, a physical space, where the equations are written regarless of the method employed for their solution; it ensues a modular structure which allows to exploit, with the same algorithm, several sets of physical data, e.g. EOS, opacity, thermonuclear reactions, diffusion, atmosphere, etc... and a few numerical parameters allow to adjust the order and the accuracy of the solution.

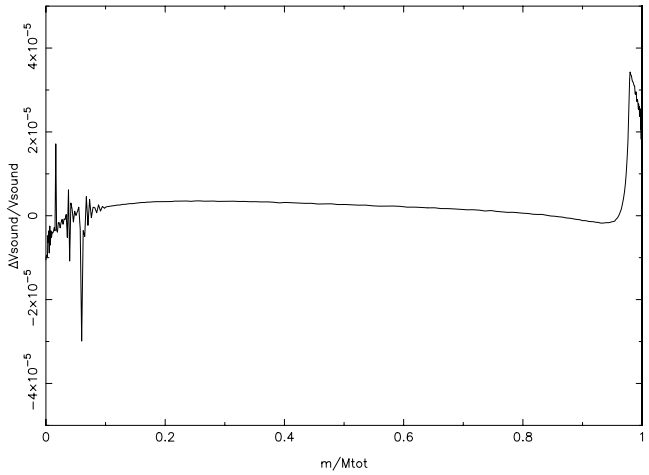

Fig. 1. Relative difference of the sound velocity between two calibrated solar models calculated with the two kinds of mixing: standard instantaneous mixing and diffusion. The low level of the differences shows that the two kinds of mixing have similar effects. The wiggly behavior for radius lesser than $0.1 M_{\rm tot}$ is a fossil signature of the discontinuities of chemicals at the limit of the convective core of the young sun; they are almost not smoothed because these calculations employed a low dissipative scheme for the interpolation of chemicals

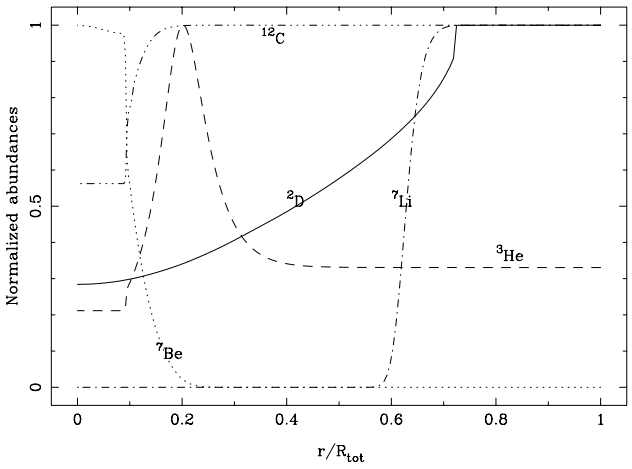

Fig. 2. Normalized abundances in a 1 $M_\odot$ non-standard model at the end of the PMS. At that age (45 My) the convective core of the young Sun recedes and the CZ is closed to its present day location. At LMR the solution is stable even if jumps of more than thirteen decades affect the diffusion coefficients. The maxima respectively are: ^{2}D $= 1.6\,10^{-17}$, ^{3}He $= 3.1\,10^{-4}$, ^{7}Li $= 4.1\,10^{-9}$, ^{7}Be $= 1.7\,10^{-12}$, ^{12}C $= 3.1\,10^{-3}$

4.1. Initializing and updating the solution

The iterative process is initialized with a model which is, either, for $t = 0$, a starting model of PMS or ZAMS or, for $t > 0$, a previously evolved model; a new initial model is then computed with the requested open parameters for physics, i.e., mass, mixing length, etc... , and for numeric, i.e., number of shells, order of piecewise polynomials etc... Along the evolution, the calculation of a new model is initialized with the previous model without extrapolation. When the gravothermal energy is the leading term in the energy equation, such as occurs during the PMS phase or with shell sources, the values for density and specific internal energy need to be accurately initialized (Kippenhahn et al. 1968); since the approximate model is the previous one, the initial value for the gravothermal energy is zero, the energy equation is strongly in error and the Newton-Raphson scheme does not converge. The remedy of Härm & Schwarzchild (1966), consists in taking the approximate model as the previous one shifted in mass; in the B-splines space, this technique is not easy to be worked out and, by experience, it does not work for PMS. A trivial solution has been found: for the first Newton-Raphson iterate, *but only for this first*, the gravothermal energy is taken equal to its value in the former model; hence the energy equation remains in almost closed form (recall that is one of the necessary conditions for the convergence of the Newton-Raphson method).

4.2. Time step controls

There are three levels of time step controls; as soon as one of the following criteria is not fulfilled the time step is divided by two, otherwise, for the next model it increases, at most, by 20%:

1. inadequate accuracy of the solution or no convergence of the IRK scheme, after more than 12 Newton-Raphson iterations,
2. slow convergence or divergence of the Newton-Raphson scheme used for the two points boundary problem,
3. too large changes in chemicals,
4. too large gravothermal energy change.

4.3. Sets of numerical parameters

The amount of calculations increases with the accuracy to be achieved, for some applications precise models are not necessarily needed, e.g. with uncertain or unstable physics; for others applications, high accuracy is reachable and is of necessity, e.g. calibrated solar models used for the calculations of frequencies; therefore the numerical parameters have to be adjusted to the aims towards the model is directed. Table 1 gathers three sets of numerical parameters of common use: i) (la) *low accuracy*, for tests, uncertain or unstable physics, ii) (sa) *standard accuracy*, iii) (Sa) *Solar accuracy*, for the calculation of precise solar models.

Table 1. Sets of numerical parameters employed for the calculation of models with: *low accuracy* (la), *standard accuracy* (sa), *Solar accuracy* (Sa) (the other notations are defined Sect. 4.3)

	(la)	(sa)	(Sa)
C	0.11	0.1	0.06
$h_{\rm c}$	2(2)	3(3)	4(3)
p	1	2	2
$(\Delta X)_{\max}$	0.3	0.2	0.1
$(\Delta t)_{\max}$	200	100	50
$h_{\rm q}$	2(2)	3(4)	3(4)
$\Delta_{\rm N}$	$5\,10^{-3}$	$1\,10^{-4}$	$5\,10^{-6}$
$\Delta_{\rm g}$	1.0	0.5	0.1
$n_{\rm a}$	25	30	50
$n_\star$	15	20	30
$n_{\rm PMS}$	250	270	450
$n_{\rm ZAMS}$	390	420	700
$n_\odot$	395	430	720

In Table 1, C is the repartition constant, $h_{\rm c}$ the order of piecewise polynomials employed for interpolation of chemicals with (in parenthesis) their values with diffusion; p is the order of the IRK scheme; $(\Delta X)_{\max}$ is the maximum relative change allowed for ^{1}H and ^{4}He during a time step of maximum length $(\Delta t)_{\max}$; $h_{\rm q}$ is the order of piecewise polynomials of the solution with (in parenthesis), their orders magnified by super convergence (see Sect. 5.2); $\Delta_{\rm N}$ is the closure used for the damped Newton-Raphson scheme; $\Delta_{\rm g}$ is the maximum relative change allowed to the gravothermal energy in the core during a time step; $n_{\rm a}$ and $n_\star$ respectively are the total number of shells in the atmosphere and between the bottom of the atmosphere and the level where the radius of the star is located; $n_{\rm PMS}$ $n_{\rm ZAMS}$, $n_\odot$ respectively are typical numbers of shells in solar model at the onset of the PMS, of the ZAMS and for the present solar age.

4.4. Calibration of solar models

The solar models are calibrated by adjusting the ratio $\alpha \equiv l/H_{\rm p}$ of the mixing-length to the pressure scale height, the initial mass fraction X of hydrogen and the initial mass fraction Z/X of heavy elements to hydrogen in order to have, at present day, the luminosity $L_\odot$, the radius $R_\odot$ and the mass fraction $\mathcal{R}_{Z\odot} \equiv (Z/X)_{t=t_\odot}$. According to Guenter et al. 1992 the most recent determinations for the solar luminosity, radius, mass and age are: $L_\odot = 3.8515\,10^{33}$ erg s^{-1}, $R_\odot = 6.9598\,10^{10}$ cm, $M_\odot = 1.9891\,10^{33}$ g, and $t_\odot = 4.52$ Gy. The value of the ratio of heavy elements to hydrogen, at present day is, $\mathcal{R}_{Z\odot} = 0.0245$ (Grevesse & Noels 1993; Noels et al. 1995).

With the microscopic diffusion coefficients of Michaud & Proffitt (1993), the following dependences on the initial PMS values of the unknown parameters has been found:

$$\begin{pmatrix} -0.6471 & -20.18 & -98.51 \\ 0.07193 & -42.50 & -222.9 \\ 2.758\,10^{-4} & 1.476\,10^{-2} & 1.016 \end{pmatrix} \begin{pmatrix} \Delta\alpha \\ \Delta X \\ \Delta\mathcal{R}_{Z0} \end{pmatrix} = \begin{pmatrix} \Delta R\,10^{10} \\ \Delta L\,10^{33} \\ \Delta\mathcal{R}_{Z\odot} \end{pmatrix}$$

with $\mathcal{R}_{Z0}$ as the value of Z/X at $t = 0$ and $\mathcal{R}_{Z\odot}$ its value at present solar age. Along the calibration process the matrix of the dependence can be updated, using the one rank Broyden's method (Conte & de Boor 1987, p. 222)

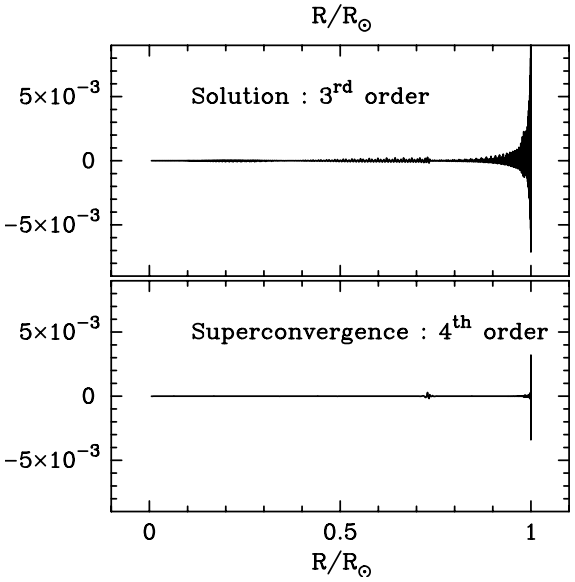

Fig. 3. Comparison of the relative accuracy on the pressure gradient between the numerical solution and its improvement taking advantage of the super convergence. Clearly one order of magnitude is acquired. One also emphasizes on the good behavior of the solution in the vicinity of the center

5. Estimates of the numerical accuracy

For results concerning external numerical tests using the simplified physics of the Solar Model Comparison project (SMC) see Christensen-Dalsgaard (1988, 1991).

5.1. Physics used for the numerical tests

Otherwise stated, the following physics is employed in numerical tests:

– EOS: EFF formalism (Eggleton et al. 1973).

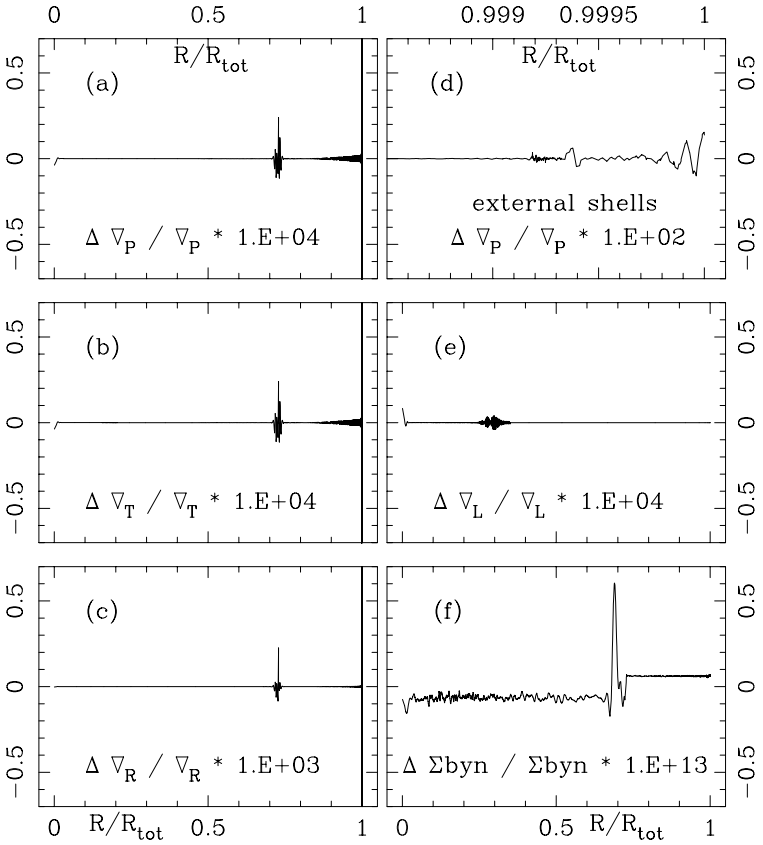

Fig. 4. Panels **a)**, **b)**, **c)**, **e)**: relative accuracy on the closure for, respectively, the first four differential equations of stellar evolution; panel **d)**: enlargement for outer layers for the pressure gradient; panel **f)**: relative difference on number of baryons. These plots are computed, using the improved solution, for more than 3500 points, randomly distributed in the model; the radius of the innermost point is $R \sim 3.8\,10^{-4} R_{\rm tot}$. The accuracy of the solution is better than $\sim 5\,10^{-6}$ except in the neighbourhood of the LMR and in the atmosphere

- Opacities: 4D linear (T_6, A, X, Z) interpolation of OPAL radiative opacity data (Rogers & Iglesias 1992) extended with Kurucz's (1991) opacity data for low temperatures; as usual, with OPAL opacity data, $T_6 \equiv T\ 10^{-6}$, $A \equiv \ln \rho / T_6^3$.
- Convection: at each level, the Schwarzchild's criterion is employed to decide if the energy transport is made by radiation or by convection. The basic formulation of the classical mixing length theory according to Henyey et al. (1965) is used for the calculation of the convective gradient; it also takes into account the optical thickness of the convective elements.
- Thermonuclear reactions: the nuclear network contains the following twelve species which enter into the most important nuclear reactions of the PP, CNO and the beginning of the 3α cycles chain (Clayton 1968): ^{1}H, ^{2}D, ^{3}He, ^{4}He, ^{7}Li, ^{8}Be, ^{12}C, ^{13}C, ^{14}N, ^{15}N, ^{16}O, ^{17}O; in some models, the species ^{2}D, ^{7}Li, ^{8}Be are assumed to be at equilibrium; the relevant nuclear reactions are interpolated from the tabulated rates of Caughlan & Fowler (1988); weak screening is assumed; the initial abundances are taken from Anders & Grevesse (1989) meteoric abundances.
- Atmosphere: single shell approximation or restoration of an atmosphere using a $\mathcal{T}(\tau)$ law derived from Kurucz's model atmospheres (Morel et al. 1994).
- Diffusion coefficient: if diffusion is not ignored, the microscopic diffusion coefficients of Michaud & Proffitt (1993) are employed.
- Angular momentum: the rotation is ignored.
- Mass loss: the mass loss is assumed to be zero and the mass defect is ignored.

5.2. Superconvergence

The expansion of the unknown functions on a basis allows to recover exactly the numerical solution at any location, i.e., *not only at the grid points*. Moreover with the de Boor's choice of the collocation points (de Boor 1978), the order of the accuracy of the numerical solution, at the grid

points, is improved[8] by *superconvergence* (see Appendix C2). This nice numerical property avoids the Richarson extrapolation (Christensen-Dalsgaard 1982) which is, with stiff problems, sometimes unstable (Hairer & Wanner 1991). That improvement is illustrated Fig. 3: for a calibrated standard solar model, evolved from the PMS to the present age with "standard accuracy" (sa), but with a *constant number of shells* fixed to 300, the relative accuracy on the pressure gradient $\frac{\partial P}{\partial M}$:

$$\left(\frac{\partial P}{\partial M} + \frac{GM}{4\pi R^4}\right) \Big/ \frac{GM}{4\pi R^4}$$

is plotted for points randomly distributed on the interval $[0, R_\odot]$; as seen, the relative precision, taking advantage of the super convergence, is improved by one order of magnitude. Figure 3 illustrates also the stability of the numerical solution near the center, the possibility of recovering, with full accuracy, the numerical solution everywhere and, the significant improvement of the accuracy in the envelope due to the superconvergence.

5.3. Estimate of the internal accuracy

For more than 3500 points randomly distributed in a model of 1 $M_\odot$, evolved from ZAMS to 4550 My, with "Solar accuracy" (Sa), the relative differences between left and right hand sides of the four first differential equations of Eq. (1), namely the derivatives $\frac{\partial P}{\partial M}$, $\frac{\partial T}{\partial M}$, $\frac{\partial R}{\partial M}$ and $\frac{\partial L}{\partial M}$, have been computed from the improved solution of fourth order; the results, plotted Fig. 4, allow an estimate of the internal accuracy achieved. That model includes an atmosphere reconstructed (see Sect. 3.2.4) and smooth opacity data have been provided using the bivariate rational spline interpolation scheme of Houdek & Rogl (1996).

As seen, the differential equations are fulfilled within a relative precision better than $\sim 5\,10^{-6}$ except in the neighbourhood of the LMR at $R \approx 0.72\ R_{\rm tot}$, and in the atmosphere for $R \gtrsim 0.9992\ R_{\rm tot}$. At LMR the local drop of the precision is a consequence of the small discontinuity of the density, caused by the mixing in the convective zone where the nuclear reactions, though weak, are active; there $\frac{\partial R}{\partial M}$ is discontinuous, the solution is only of class $\mathcal{C}^0$, the fourth order accuracy cannot be reached; the effect is more sensitive for $\frac{\partial R}{\partial M}$ than for the other gradients, Fig. 4 panel (c). The cause of the low accuracy $\sim 2\,10^{-3}$ in the restored atmosphere, panel (d), is a consequence of the non-linear dependence of the *natural* variable τ, used for the restoration of the atmosphere, with respect to R through the $\mathcal{T}(\tau)$ law and the opacity.

In the model, the closest grid point from the center is located at $R \sim 1.2\,10^{-2} R_{\rm tot}$; in the plots, deliberately, the first point was located at $R \sim 3.8\,10^{-4} R_{\rm tot}$, i.e., quite near to the central singularities; the stability of the numerical solution there is clearly illustrated Fig. 4, panels (a), (b) (c) and (e).

[8] Only where the true solution is sufficiently smooth.

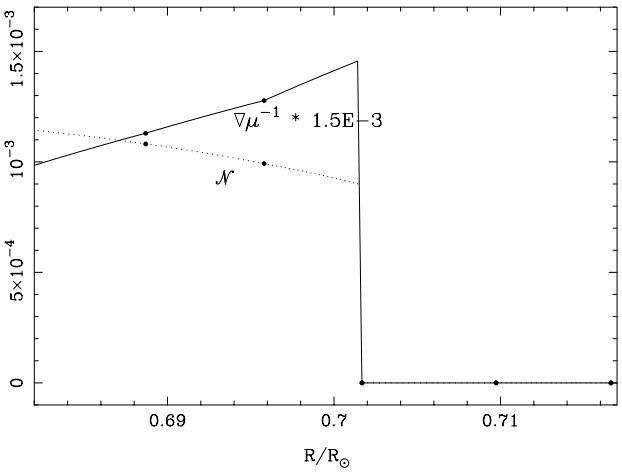

Fig. 5. Plots, with respect to the normalized radius, of discontinuous quantities $\mathcal{N}$ (dots) and $\partial\mu^{-1}/\partial R$ (full) – μ is the mean molecular weight – in the neighbourhood of the LMR of a solar model with microscopic diffusion; on the $\mathcal{N}$ curve, between two grid points (•), each dot corresponds to a *calculated* and not to an interpolated value of $\mathcal{N}$

As demonstrated Appendix B4 and Appendix C4, the algorithm employed for the calculation of the chemical composition are conservative; that is illustrated Fig. 4 panel (f), where the local departure from the mean value of the number of baryons, $\sum_{i=1}^{n_X} \frac{n_i}{A_i} X_i$ is plotted; n_i and A_i are, respectively, the baryonic number and the atomic weight of X_i. As seen, the conservation of the number of baryon is ensured within the machine accuracy except at LMR, due to the mixing which is not made with so high numerical accuracy (see Sect. 3.3.2) and, also to the displacement of the LMR.

5.4. Discontinuities

Figure 5 illustrates the ability to restore the solution at any location, even with discontinuous functions. Due to the convective mixing, in a stellar model taking diffusion into account the gradient of the mean molecular weight (here noted μ) and the quantity:

$$\mathcal{N}^2 \equiv \frac{GM}{R^2}\left(\frac{1}{\Gamma_1}\frac{\partial \ln P}{\partial R} - \frac{\partial \ln \rho}{\partial R}\right),$$

are discontinuous at LMR – $\mathcal{N}$, difference between two gradients, is equivalent to a second derivative – Γ_1 is the adiabatic exponent. In the neighbourhood of the LMR of a model[9] with microscopic diffusion (Michaud & Proffitt

[9] This calibrated solar model was evolved, using standard accuracy (sa), from PMS to present solar age with no chemical at equilibrium, a reconstructed atmosphere and an undershooting of 0.2 pressure scale height.

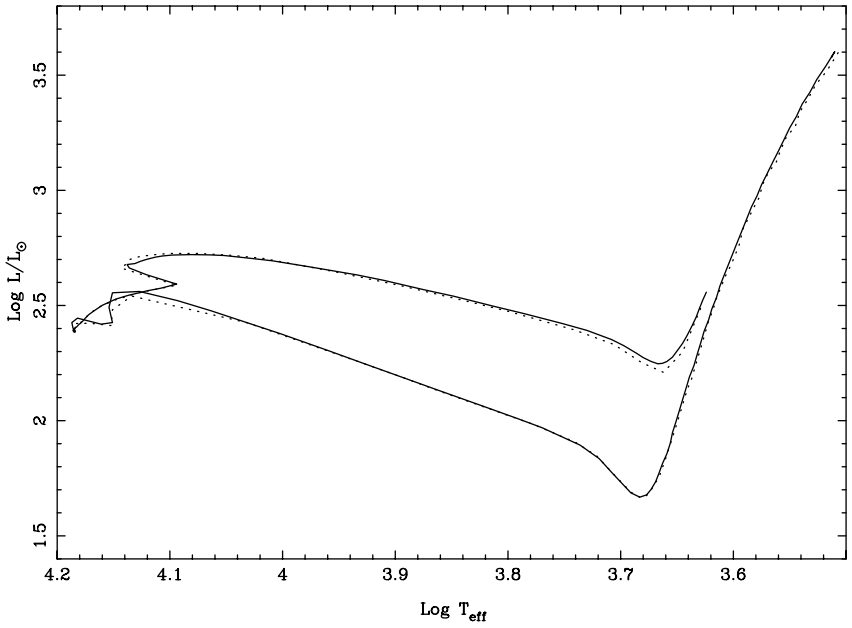

Fig. 6. Evolutionary tracks of two 4 $M_\odot$ models computed with low (dotted) and super (full) accuracy from PMS initial conditions to the onset of the 3α cycle. Large time steps are responsible of the angular behavior of the solution of low accuracy; the two tracks do not significantly differ, they are superimposed on the main sequence

1993), the above discontinuous functions have been derived from the solution, taking advantage of the superconvergence; in Fig. 5 more than 20 point are inserted between two adjacent grid points. Emphasize is made on the following facts: i) the discontinuity is well marked, ii) in its vicinity, even with jumps, for the diffusion coefficients, as large as thirteen magnitudes, the solution has no oscillation, iii) $\mathcal{N}$, a second derivative, is smooth, iv) a grid point is placed right on the LMR.

5.5. Comparison of evolutionary tracks

Two models of 4 $M_\odot$ have been evolved starting from PMS to the onset of the ^{4}He burning phase; these two models differ only by the numerical accuracy achieved. The first one, is computed with low accuracy (la), the second with standard accuracy (sa), see Table 1; the numbers of, time steps, shells at the onsets of PMS, ZAMS, POST and 3α cycle burning phase, are given Table 2. The evolutionary tracks are notably stable, even for the rugged solution obtained with (la); notice also that, on the main sequence, the two tracks are superimposed.

Table 2. Typical number of shells used in the calculations of 4 $M_\odot$ models with, respectively, low (la) and standard (sa) accuracy

	(la)	(sa)
$n_{\Delta t}$	103	137
$n_{\rm PMS}$	250	270
$n_{\rm ZAMS}$	420	460
$n_{\rm POST}$	430	480
$n_{3\alpha}$	480	530

6. Discussion

The principal novel feature of the CESAM code, devoted to the calculation of stellar evolution, is the assumption that the dependent variables can be approached by piecewise polynomials which are, in turn, projected on a convenient basis for the numerical analysis; that allows to handle the discontinuities without too much difficulties, to have a scheme with an order of accuracy having only one parameter dependence and the possibility of improving the numerical solution via the super convergence.

Other unusual features are the use of i) an automatic location of the numerical mesh with a variable total number of points and adjustment of grid points in close neighborhoods of each limit of convective zones, ii) a stiffly stable implicit Runge-Kutta scheme with orders up to four for the computation of the chemicals change, iii) finite elements approach for the calculation of diffusion, using Petrov-Galerkin formalism with a large turbulent diffusion for mixing the chemicals in convective zones, iv) precise reconstitution of the atmosphere with the stellar radius located at the level where the local temperature is equal

to the effective temperature, v) mass changes due to the mass loss and mass defect are also allowed for.

The linearized equations are solved using the damped Newton-Raphson that allows to follow evolution with good time steps and reduced nets, even with shell sources. Although the set of lagrangian variables used so far allows to reach the best numerical accuracy, it does not permit to pursue the evolution towards more advanced phases if negative values of the local luminosity are expected; in such cases the calculations are possible with a numerically, less accurate set of eulerian variables.

The most constraining features are i) the use of the pressure, instead of the density, as state variable and ii) the necessity, for all the physical quantities, of numerically consistent derivatives with respect to the variables of state, i.e., pressure, temperature and chemical composition.

The extension of this code towards more advanced stages of stellar evolution is under investigations.

Acknowledgements. I acknowledge the suggestion by E. Schatzman and A. Baglin to undertake the development of this code; J. Provost and G. Berthomieu for advices, debugging and constructive criticisms of the results; J. Christensen-Dalsgaard, M. Gabriel, A. Noels, J. Reiter for stimulating and helpful discussions; C. van't Veer, Y. Lebreton, M.J. Goupil and my colleagues of GDR CNRS 131 for various contributions to CESAM. I wish to express my thanks to the anonymous referee whose comments and remarks greatly helped to improve the presentation of this paper.

References

Alecian G., 1986, A&A 168, 204
Anders E., Grevesse N., 1989, Geoch. Cosmoch. Acta 53, 197
Arnett W.D., Truran J.W., 1969, ApJ 157, 339
Audard N., Provost J., 1994, A&A 282, 73
Berthomieu G., Provost J., Morel P., Lebreton Y., 1993, A&A 268, 775
de Boor C., 1978, A Practical Guide to Splines Springer, third edition 1985
de Boor C., Swartz B., 1973, SIAM J. Numer. Anal. 10, 582
Bressan A., Fagotto F., Bertelli G., Chiosi C., 1993, A&AS 100, 647
Caughlan G.R., Fowler W.A., 1988, Atom. Data Nucl. Data Tab. 40, 284
Clayton D.D., 1968, Principles of Stellar Evolution and Nucleosynthesis. Mc Graw–Hill
Charbonel C., Vauclair S., Zahn J.P., 1992, A&A 255, 191
Chmielewski Y., Cayrel de Strobel G., Cayrel R., Lebreton Y., Spite M., 1995, A&A 299, 809
Christensen-Dalsgaard J., 1982, MNRAS 199, 735
Christensen-Dalsgaard J., 1988, Computational procedures for GONG solar model project, Astronomisk Institut, Aarhus Universitet
Christensen-Dalsgaard J., 1991, Solar oscillations and the physics of the solar interior. Challenges to Theories of the Structure of Moderate-Mass Stars. In: Gough D.O. and Toomre J. (eds.). Springer Verlag, p. 11
Clayton D.D., 1968, Principles of Stellar Evolution and Nucleosynthesis. Mc Graw–Hill
Conte S.D., de Boor C., 1987, Elementary Numerical Analysis. McGraw-Hill Book Company, third edition
Cox A.N., Guzik J.A., Kidman R.B., 1989, ApJ 342, 1187
Eggleton P., 1971, MNRAS 151, 351
Eggleton P., 1972, MNRAS 156, 361
Eggleton P., Faulkner J., Flannery B.P., 1973, A&A 23, 325
Embarek B., 1989, Stage de Maitrise d'Ingénierie mathématique, Université de Nice, juin 1989
Gabriel M., 1990, in Progress of seismology of the sun and stars, Osaki Y. and Shibahashi H. (eds.). Springer, New York, p. 23
Gaches J., 1988, Modélisation de Courbes et surfaces Splines, Ecole Nationale Supérieure d'Ingénieurs de Constructions Aéronautiques, Toulouse
Gear C.W., 1971, Numerical initial value problems in ordinary differential equations. Prentice Hall
Goupil M.J., Michel E., Lebreton Y., Baglin A., 1993, A&A 268, 546
Grevesse N., Noels A., 1993, in Origin and Evolution of the Elements. In: Prantzos N., Langioni-flam E., Casse M. (eds.). Cambridge Univ. Press, p. 14
Guenther D.B., Demarque P., Kim Y.C., Pinsonneault M.H., 1992, ApJ 387, 372
Guillot T., Morel P., 1995, A&AS 109, 109
Hairer E., Wanner G. 1991, Solving Ordinary Differential Equations II. Springer-Verlag
Han Z., Podsiadlowski P., Eggleton P.P., 1994, MNRAS 270, 121
Härm R., Schwarzchild M., 1966, ApJ 145, 1966
Henyey L.G., Le Levier R., Levee R.D., 1959, ApJ 129, 2
Henyey L.G., Forbes J.E., Goult N.L., 1964, ApJ 139, 306
Henyey L.G., Vardya M.S., Bodenheimer P.L., 1965, ApJ 142, 841
Houdek G., Rogl J., 1996, Bull. Astr. Soc. India 24, 317
Iben I., 1975, ApJ 196, 525
Kippenhahn R., Weigert A., Hofmeister E., 1968, Meth. Comput. Phys. 7, 129
Kippenhahn R., Weigert A., 1991, Stellar Structure and Evolution. Springer-Verlag
Kurucz R.L., 1991, Stellar Atmospheres: Beyond Classical Models, Crivellari L., Hubeny I. and Hummer D.G. (eds.), NATO ASI Series. Kluwer, Dordrecht 1991
Lebreton Y., Michel E., Goupil M.J., Baglin A., Fernandes J., 1995, Accurate parallaxes and stellar ages determinations IAU Symp. 166, La Haye, August 1994. Hoeg E., Seidelmann P.K. (eds.). Dordrecht: D. Reidel, p. 135
Maeder A., Meynet G., 1987, A&A 182, 243
Marchouk G., Agochkov V., 1985, Méthode des Eléments Finis, Mir
Michaud G., Proffitt C.R., 1993, Inside the Stars, IAU colloquium 137, Weiss W.W. and Baglin A. (eds.) ASP Conf. Ser. 40, 246
Mihalas D., 1978, Stellar Atmosphere, 2d Edition. Freeman and Cie
Mihalas D., Däppen W., Hummer D.G., 1988, ApJ 331, 815
Morel P., 1989, Un code d'Evolution Stellaire Adaptatif et Modulaire, Cours de Structure Interne, Ecole d'Aussois, Hubert A.M. and Schatzman E. (eds.). Publ. Obs. Paris Sect. Meudon

Morel P., Provost J., Berthomieu G., 1990, Solar Phys. 282, 73
Morel P., van't Veer C., Berthomieu G., et al., 1993, Inside the Stars, Weiss W.W. and Baglin A. (eds.) IAU Colloquium 137, p. 57
Morel P., 1993a, Utilisation et description du Code d'Evolution Stellaire CESAM, Pub. Obs. Nice
Morel P., 1993b, Inside the Stars, Weiss W.W. and Baglin A. (eds.) IAU Colloquium 137, p. 445
Morel P., van't Veer C., Provost, 1994, A&A 286, 91
Morel P., Schatzman E., 1996, A&A 310, 982
Noels A., Grevesse N., Mazzitelli I., 1995, Processes in Astrophysics, International meeting in honour of Evry Schatzman, Roxburg I.W. and Masnou J.L. (eds.) Lecture Notes in physics. Springer, p. 203
Paczynski B., 1969, Acta Astron. 19, 1
Press W.H., Flannery B.P., Teukolsky S.A., Vetterling W.T., 1986, Numerical Receipes, Cambridge University Press. Cambridge
Proffitt C.R., Michaud G., 1991, ApJ 371, 584
Quarteroni A., Valli A., 1994, Numerical approximation of partial differential equations. Springer-Verlag
Reiter J., Bulirsh R., Pfleiderer J., 1994, Astron. Nachr. 315, 205
Reiter J., Walsh L., Weiss A., 1995, MNRAS 274, 899
Richtmyer R.D., Morton K.W., 1967, Finite Differences Methods for Initial Values Problems, 2d. Edt. Intersciences Publishers, New-York
Rogers F.J., Iglesias C.A., 1992, ApJS 79, 507
Rossignol S., 1995, Mémoire de DEA, Astronomie, Imagerie et Haute Résolution Angulaire. Université de Nice-Sophia Antipolis
Schatzman E., 1959, Sur la perte de masse et les processus de freinage de la rotation, I.A.U. Symposium 10, Greenstein J. (ed.) Ann. Astr. Supp. 8, 129
Schatzman E., Maeder A., Angrand F., Glowinski R., 1981, A&A 96, 1
Schatzman E., Praderie F., 1990, Les Etoiles, InterEditions/ Editions du CNRS
Schumaker L., 1981, Splines Functions: Basic Theory, John Whiley
Stoer J., Bulirsch R., 1979, Introduction to Numerical Analysis. Springer-Verlag
Strittmatter P.A., Faulkner J., Robertson J.W., Faulkner D.J., 1970, ApJ 161, 369
Wagoner R.V., 1969, ApJS 18, 247
Wilson R.E., 1981, A&A 99, 43
Zahn J.P., 1991, A&A 252, 179